Letter | Editors' Suggestion

Giant density fluctuations in locally hyperuniform states

Sara Dal Cengio [1,2,*] Romain Mari [2] and Eric Bertin [2]

[1]*Department of Physics, Massachusetts Institute of Technology, Cambridge, Massachusetts 02139, USA*

[2]*Université Grenoble Alpes, CNRS, LIPhy, 38000 Grenoble, France*

(Received 23 October 2024; revised 14 March 2025; accepted 12 September 2025; published 14 October 2025)

Systems driven far from equilibrium may exhibit anomalous density fluctuations: active matter with orientational order displays giant density fluctuations at a large scale, while systems of interacting particles close to an absorbing phase transition may exhibit hyperuniformity, suppressing large-scale density fluctuations. We show that these seemingly incompatible phenomena can coexist in nematically ordered active systems, provided activity is conditioned to particle contacts. We characterize this unusual state of matter and unravel the underlying mechanisms simultaneously, leading to spatially enhanced (on large length scales) and suppressed (on intermediate length scales) density fluctuations. Our work highlights the potential for a rich phenomenology in active matter systems in which the particles' activity is triggered by their local environment, and calls for a broader exploration of absorbing phase transitions in orientationally ordered particle systems.

DOI: 10.1103/m6bl-dqsd

Outside critical points, particle systems at thermal equilibrium have a finite compressibility and display normal density fluctuations in homogeneous phases. By contrast, athermal systems of polydisperse particles such as disordered sphere packings [1,2], dense emulsions [3], and colloidal suspensions [4] may display hyperuniformity, whereby large length-scale density fluctuations are suppressed [5–8]. For monodisperse athermal particle systems, hyperuniformity is often observed at the critical point of an absorbing phase transition [9–15] (although not always [16]). Physical realizations include cyclically sheared suspensions [12,17–19], whose stroboscopic dynamics has been schematically described by the Random Organization Model (ROM) [9,10,17,20], as well as some systems of active particles [21,22], or topological defects in active nematics [23]. Hyperuniform regimes have also been reported in systems with long-range (e.g., hydrodynamic) interactions (such as chiral active particles [24], spinners or vortices in a fluid [25], or microvortices in active turbulence [26]), or short-range antialigning interactions [27]. Finally, clustering or coarsening patterns lead to hyperuniformity on very large length scales in scalar active matter [28–30], where no large-scale orientational order develops.

By contrast, systems of orientationally ordered active particles are notoriously characterized by giant number fluctuations (GNFs). Large length-scale density fluctuations exceed the ones of an equilibrium system, due to the slow decay of the two-point density correlation function which arises from coupling with orientational order [31,32]. GNFs occur without the fine tuning of parameters and are predicted to appear generically in the orientationally ordered phase of active matter. GNFs were first predicted using fluctuating hydrodynamics [31], and afterwards observed in numerical [33–35] and experimental realizations, including vibrated rods [36], vibrated polar disks [37], bacteria colonies [38], and epithelial cells [39].

It is thus of interest to quantitatively characterize the density fluctuations in a system which mixes the key ingredients to GNFs and hyperuniformity. Indeed, many active particle systems can potentially exhibit orientational order (e.g., due to alignment interactions) and an absorbing phase transition (e.g., due to a motility that is activated by the presence of neighbors). Experimentally feasible systems may include suspensions of rodlike particles under cyclic shear near their reversible-irreversible transition [40,41], Quincke rollers with neighbor-triggered motility [42], assemblies of biological cells with stress-induced motility [43,44], collections of active microtubules [45], or swarms of macro- [46] or microrobots [47,48]. Understanding how the interplay of interaction-triggered motility and orientational order impacts large-scale density fluctuations may thus open avenues for designing active systems with self-organized complex states.

In this Letter, we introduce an active nematics model exhibiting an absorbing phase transition similar to the one of the ROM, that we refer to as the nematic ROM (NROM). This minimal model is inspired by experiments on cyclically sheared suspensions of rods [40,41] and on subcritical Quincke rollers [42], both which display neighbor-triggered motility and orientational ordering. We show that when the absorbing phase transition occurs in the nematically ordered state, the system dynamically organizes to suppress density fluctuations in an intermediate range of length scales when approaching the transition, and to enhance fluctuations at larger length scales, where GNFs are observed. We predict a critical crossover between these two anomalous regimes of density fluctuations, which we characterize using a continuum theory. In this framework, the crossover arises from the competition between two effective noises on the density field. More generally, our results open avenues for future research on the detailed characterization of universality classes of absorbing

*Contact author: saradc@mit.edu

phase transitions in active matter with orientational order and environment-triggered motility.

We consider a two-dimensional (2D) system of N particles with diameter D in a box of linear size L and periodic boundary conditions. Each particle $i = 1, \ldots, N$ at position $\boldsymbol{r}_i^t$ carries an axial direction $\theta_i^t \in [-\pi/2, \pi/2]$ and aligns noisily to the neighboring particles within the interaction range $R_{\rm al}$. At each time step, the directors $\boldsymbol{n}_i^t = (\cos\theta_i^t, \sin\theta_i^t)$ are updated according to a Vicsek-type active nematics rule [33,35],

$$\theta_i^{t+1} = \frac{1}{2}\arg\left[\sum_{k\in\mathcal{V}_i} e^{\mathrm{i}2\theta_k^t}\right] + \psi_i^t \mod \pi, \tag{1}$$

where $\mathcal{V}_i$ is the neighborhood of particle i and $\psi_i^t \in [-\sigma\pi/2, \sigma\pi/2]$ is a random angle drawn from a uniform distribution, with $\sigma \in [0, 1]$ the noise intensity. Unlike usual active nematics models [33,35] where all particles permanently diffuse, here only particles overlapping with another particle (i.e., with a center-to-center distance smaller than D) are motile. The position of overlapping particles is updated as

$$\boldsymbol{r}_i^{t+1} = \boldsymbol{r}_i^t \pm \delta_0 \boldsymbol{n}_i^t, \tag{2}$$

with random equiprobable signs, and δ_0 a fixed step size. Our model thus generalizes the Vicsek-type active nematics model [33,35] to a ROM-type model with nematic interactions and anisotropic diffusion, such that particles diffuse along their individual director $\boldsymbol{n}_i^t$, only when in overlap with another particle (however, all angles θ_i are updated at each time step). The NROM boils down to the ROM for maximal angular noise ($\sigma = 1$), while active nematics is recovered for $D \to \infty$ (interpreting D as an interaction range for triggering motion).

We start by recalling the schematic phase diagrams of the ROM and active nematics models. The control parameters of the ROM are the packing fraction $\phi = \frac{N\pi D^2}{4L^2}$ and the step size δ_0. Its phase diagram is sketched in Fig. 1(a): A passive phase at small ϕ for which the system always falls into an absorbing state after a finite number of time steps is separated from an active phase at large ϕ by an absorbing phase transition (purple line). The control parameters of the Vicsek-type active nematics model [33,35] are the dimensionless density $\rho = \frac{NR_{\rm al}^2}{L^2}$ and the noise intensity σ [Eq. (1)]. An isotropic state is obtained for large noise and small density, while nematic order sets in for small noise and large density [Fig. 1(b)], with a phase-separated region close to the transition.

The combined model (NROM) has four control parameters, and therefore a potentially complex phase diagram. However, we aim at a restricted region within this phase diagram: close to the absorbing phase transition where hyperuniformity could arise (i.e., for ϕ around the critical packing fraction $\phi_{\rm c}$) in an otherwise nematically ordered phase showing GNFs (i.e., for large ρ). These two conditions can be simultaneously satisfied for $D/R_{\rm al}$ smaller than a threshold value that depends on σ and δ_0 values. Here, we use $\sigma = 0.1$, $\delta_0 = 0.3$, $R_{\rm al} = 1$, and pick $D = 0.46$ [49]. The system size is $L = 516$ unless otherwise specified, and simulations are initialized with random uniformly distributed positions and angles.

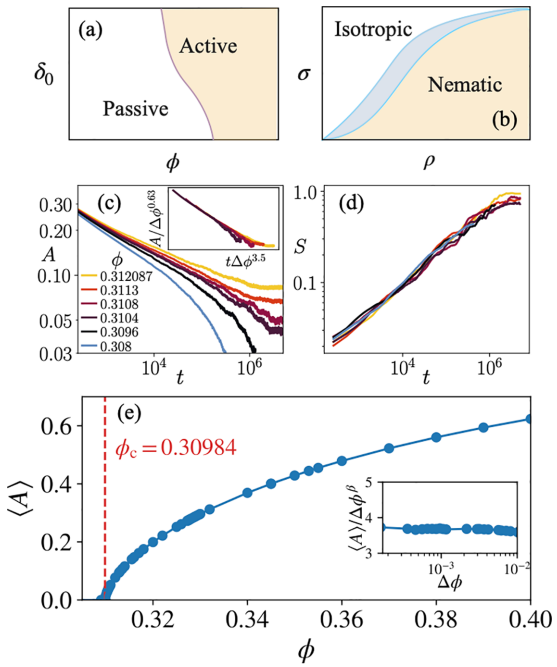

FIG. 1. (a) Sketch of the phase diagram for the ROM model showing the active and passive phases in the volume fraction ϕ–step size δ_0 plane, inspired by Fig. 1 in Ref. [10]. (b) Sketch of the phase diagram for active nematics showing the isotropic and nematically ordered phases in the density ρ–noise amplitude σ plane, inspired by Fig. 2 in Ref. [35] (blue shaded area: phase-separated nematic state). The NROM model: (c) Activity A (data collapse shown in the inset) and (d) scalar nematic order S vs time, for several packing fractions ϕ. Data are averaged over more than 40 realizations. (e) Steady-state activity $\langle A \rangle$ vs packing fraction ϕ.

We show in Fig. 1(c) the activity A, defined as the fraction of active (i.e., overlapping) particles, as a function of time. An absorbing phase transition is observed at a packing fraction $\phi_{\rm c}$. For $\phi > \phi_{\rm c}$, the activity reaches a steady state around an averaged value $\langle A \rangle > 0$ in a time that diverges when $\phi \to \phi_{\rm c}^+$ [see Fig. 1(c) inset]. By contrast, for $\phi < \phi_{\rm c}$, the activity dies out in a finite time, and particle positions become frozen. In Fig. 1(e), we show $\langle A \rangle$ as a function of ϕ and the corresponding critical behavior $\langle A \rangle / \Delta\phi^\beta$ vs $\Delta\phi = \phi - \phi_{\rm c}$, from which we estimate $\phi_{\rm c} = 0.309\,84 \pm 0.000\,06$. A fit yields an exponent $\beta \approx 0.63 \pm 0.01$ [Fig. 1(e)], a value compatible with the two-dimensional conserved directed percolation (CDP) class [50], the universality class of absorbing phase transition to which the ROM belongs [18,51,52]. In addition, the traceless nematic tensor is defined as $\boldsymbol{Q} = N^{-1}\sum_i \boldsymbol{n}_i^t \boldsymbol{n}_i^t - \frac{1}{2}\mathbf{1}$, with $\mathbf{1}$ the identity matrix, and the nematic scalar order parameter reads $S = 2\sqrt{|\det \boldsymbol{Q}|}$ ($0 \leqslant S \leqslant 1$). For $\phi > \phi_{\rm c}$, the system reaches a highly ordered nematic state with $S > 0.9$ [Fig. 1(d)] within a time which does not diverge at $\phi_{\rm c}$ (for $\phi < \phi_{\rm c}$, the simulation is stopped when falling into an absorbing state). In the following, we focus on the case $\phi > \phi_{\rm c}$.

To characterize density fluctuations, we evaluate the variance $\langle \Delta n^2 \rangle_\ell = \langle n^2 \rangle_\ell - \langle n \rangle_\ell^2$ of the particle number n within boxes of different linear size ℓ. We plot in Fig. 2(a) the variance $\langle \Delta n^2 \rangle_\ell$ vs $\langle n \rangle_\ell$, parametrized by the box size ℓ, for different ϕ close to the critical point. Normal

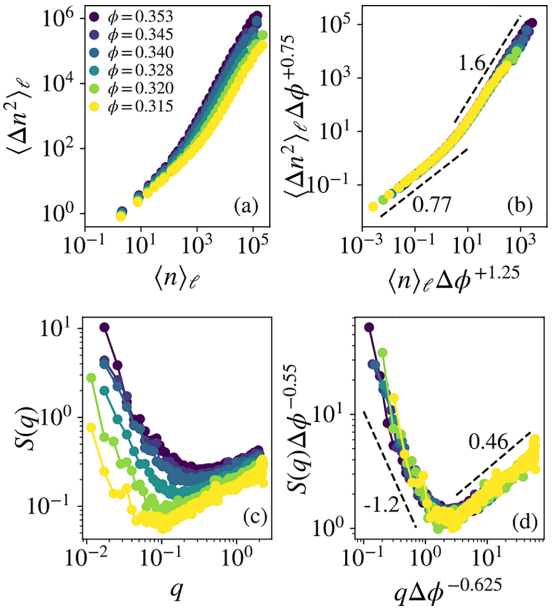

FIG. 2. (a) Number fluctuations $\langle \Delta n^2 \rangle_\ell = \langle n^2 \rangle_\ell - \langle n \rangle_\ell^2$ vs $\langle n \rangle_\ell$ in logarithmic scale for several packing fractions $\phi > \phi_c = 0.309\,84$. (b) Same data, rescaled as $\langle \Delta n^2 \rangle_\ell / \Delta\phi^{-0.75}$ vs $\langle n \rangle_\ell / \Delta\phi^{-1.25}$. (c) Structure factor $S(q)$ for several values of $\phi > \phi_c$ in logarithmic scale. (d) Same data, rescaled as $S(q)/\Delta\phi^{0.55}$ vs $q/\Delta\phi^{0.625}$. For $\phi = 0.353, 0.345, 0.340, 0.328$, the system size is $L = 516$, and for $\phi = 0.320, 0.315$, the system size is $L = 774$.

fluctuations follow a power law $\langle \Delta n^2 \rangle_\ell \sim \langle n \rangle_\ell^\alpha$ with $\alpha = 1$, while $\alpha > 1$ corresponds to GNFs [31,33,35], and $\alpha < 1$ corresponds to hyperuniformity [6,9]. We identify two distinct regimes of anomalous density fluctuations: at intermediate length scales the system develops hyperuniformity ($\alpha = \alpha_{\rm hu} = 0.77 \pm 0.005$, consistent with the value found in the ROM [9]), while for large length scales the system displays GNFs ($\alpha = \alpha_{\rm gnf} = 1.65 \pm 0.05$, as found in the 2D nematic Vicsek model [35]) [see Fig. 2(a)]. The crossover length ξ between the two regimes grows when approaching the critical point ($\phi \to \phi_c^+$). We assume a power-law scaling $\xi \sim \Delta\phi^{-\mu}$ (with μ to be determined), corresponding to a characteristic number of particles $n^* = \rho\xi^2 \sim \Delta\phi^{-2\mu}$. This critical scaling suggests a possible data collapse by plotting $\langle \Delta n^2 \rangle_\ell \Delta\phi^\zeta$ vs $\langle n \rangle_\ell \Delta\phi^{2\mu}$, under appropriate choices of the exponents μ and ζ. We find a good data collapse for $\mu = 0.625 \pm 0.02$ and $\zeta = 0.75 \pm 0.05$ [Fig. 2(b)]. The divergence of the crossover length ξ at ϕ_c shows that by getting close enough to the critical point, one may observe hyperuniformity on arbitrarily large length scales.

Density fluctuations are usually also characterized with the structure factor $S(\boldsymbol{q}) = N^{-1} \langle \sum_{i,j} e^{i\boldsymbol{q}\cdot(\boldsymbol{r}_i - \boldsymbol{r}_j)} \rangle$, which is experimentally accessible for systems of interest [53]. Since $S(\boldsymbol{q})$ may be anisotropic due to the nematic order, we introduce the angular averaged structure factor $S_{\rm iso}(q)$ with $q = |\boldsymbol{q}|$. For small $q \ll 2\pi/D$, $S_{\rm iso}(q)$ maps to $\langle \Delta n^2 \rangle_\ell$ [6]:

$$S_{\rm iso}(q) \sim \frac{\langle \Delta n^2 \rangle_\ell}{\langle n \rangle_\ell} \quad \text{with} \quad q \sim \frac{2\pi}{\ell}. \tag{3}$$

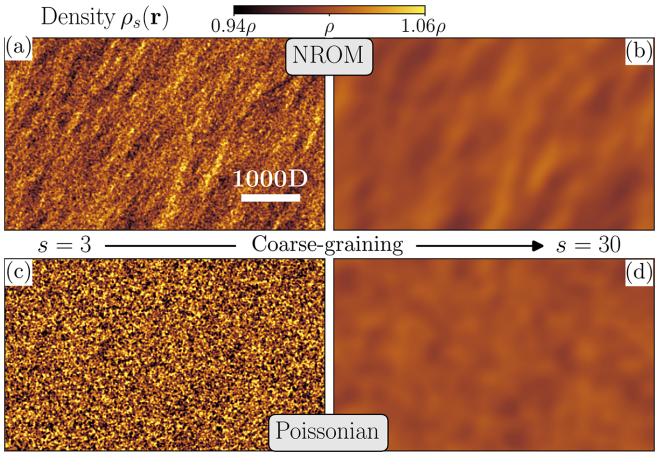

FIG. 3. Density fields of steady-state configurations from the NROM model [top row, (a) and (b)] and of a Poissonian realization [bottom row, (c) and (d)] with the same system size $L = 2850$ and packing fraction $\phi = 0.343\,27$, obtained with two different values of the coarse-graining length s: $s = 3$ [(a) and (c)] and $s = 30$ [(b) and (d)].

If $\langle \Delta n^2 \rangle_\ell \sim \langle n \rangle_\ell^\alpha$, then $S_{\rm iso}(q) \sim q^\lambda$ for small q, with $\lambda = (1 - \alpha)d$ [6], with d the space dimension. For the 2D Manna model (a lattice sandpile model in the CDP class [54]), this relation gives $\lambda_{\rm hu} \approx 0.46$, corresponding to hyperuniformity [13]. In contrast, for 2D active nematics this gives $\lambda_{\rm gnf} \approx -1.2$, leading to GNFs. We plot on Fig. 2(c) the structure factor evaluated numerically for the same values of ϕ as in Fig. 2(a). We again find two scaling regimes. For very small q, we observe a divergence compatible with a power law $q^{\lambda_{\rm gnf}}$, with $\lambda_{\rm gnf} < 0$. For intermediate values of q, we rather observe a power law $q^{\lambda_{\rm hu}}$ with $\lambda_{\rm hu} > 0$. We obtain a data collapse under an appropriate rescaling [Fig. 2(d)], by plotting $S_{\rm iso}(q)/\Delta\phi^{\zeta'}$ vs $q/\Delta\phi^\mu$ with $\zeta' = 0.55 \pm 0.05$ and $\mu = 0.625 \pm 0.05$ [same value of μ as in Fig. 2(b)], thereby confirming the critical crossover between hyperuniformity and GNFs around a wave number $q^* \sim \xi^{-1} \sim \Delta\phi^\mu$. Using $\langle n \rangle_\ell \sim \ell^2 \sim q^{-2}$, Eq. (3) yields $\zeta' = 2\mu - \zeta \approx 0.5$, which is compatible with our numerical estimate. The behavior of the structure factor, with giant density fluctuations on length scales up to system size, highlights the role of nematic order. By contrast, for $\phi < \phi_c$, where nematic ordering does not have time to build up, a crossover to normal fluctuations is observed at $q \to 0$ [55], just as in the usual ROM [14,18].

To illustrate the coexistence of different density fluctuation regimes, we compare in Fig. 3 the density fields $\rho_s(\boldsymbol{r}) = (2\pi s^2)^{-1} \sum_i \exp[-(\boldsymbol{r} - \boldsymbol{r}_i)^2/2s^2]$ obtained from the same steady-state particle configuration under two values of the coarse-graining length s [Figs. 3(a) and 3(b)] to a random (Poissonian) particle configuration [Figs. 3(c) and 3(d)]. Compared to the random configuration, the NROM density field appears comparably smoother (more uniform) than the random configuration for small s, illustrating hyperuniformity, whereas it shows fluctuations of larger amplitude and length scales for large s that are consequences of GNFs.

To get some insight on the crossover length ξ, we introduce a hydrodynamic description based on the three relevant physical fields: the particle density $\rho(\boldsymbol{r}, t)$, the nematic

tensor field $\boldsymbol{Q}(\boldsymbol{r},t)$, and the activity field $A(\boldsymbol{r},t)$ defined as the density of overlapping particles. Particles move only when they are active, so the same particle current $\boldsymbol{J}$ appears in the evolution equations for ρ and A. In a gradient expansion, the most general deterministic part of the particle flux is $\boldsymbol{J} = D_\rho \nabla A + \chi_1 \boldsymbol{Q}\cdot\nabla A + \chi_2 A \nabla\cdot\boldsymbol{Q}$, where $D_\rho > 0$, and χ_1 and χ_2 are parameters. The last two terms represent curvature-driven currents, specific of active nematics. The continuity equation for the (conserved) density field reads

$$\partial_t \rho = \nabla\cdot(\boldsymbol{J} + \sigma_\rho\sqrt{A}\boldsymbol{\eta}_\rho), \tag{4}$$

with σ_ρ a positive parameter and $\boldsymbol{\eta}_\rho(\boldsymbol{r},t)$ a vectorial unit Gaussian white noise, $\langle\boldsymbol{\eta}_\rho(\boldsymbol{r},t)\boldsymbol{\eta}_\rho(\boldsymbol{r}',t')\rangle = \delta(\boldsymbol{r}-\boldsymbol{r}')\delta(t-t')\mathbf{1}$. We assume the same reaction terms for the activity as in the CDP universality class [51,56], so that

$$\partial_t A = \nabla\cdot\boldsymbol{J} + (\kappa\rho - a)A - \lambda A^2 + \sigma_A\sqrt{A}\eta_A, \tag{5}$$

where κ, a, λ, σ_A, are positive parameters, and $\eta_A(\boldsymbol{r},t)$ is a scalar unit Gaussian white noise. The reaction terms in Eq. (5) account for the fact that the activity field A is not conserved: upon a random displacement, an active particle may become passive, or may activate a passive particle by overlapping with it. Moreover, A is nonzero in stationary state only for $\rho > \rho_c$. The noise on particle current is neglected with respect to the nonconserved noise. The effect of the nematic field $\boldsymbol{Q}$ is limited to the transport term $\nabla\cdot\boldsymbol{J}$, and is the only difference with the usual CDP dynamics for A. To lighten the presentation, we set here $\chi_1 = 0$ in $\boldsymbol{J}$, which has no qualitative effect on the density fluctuation crossover (the full calculation with $\chi_1 \neq 0$ is given in the Supplemental Material [55]). Particles align with their neighborhood irrespective of their activity, but nematic order is transported only by diffusion of active particles, yielding the following evolution for the nematic tensor,

$$\partial_t \boldsymbol{Q} = [\tilde{\mu}(\rho) - \gamma|\boldsymbol{Q}|^2]\boldsymbol{Q} + D_Q\nabla^2\boldsymbol{Q} + \chi_3\widehat{\nabla\nabla}A + \sigma_Q\boldsymbol{\eta}_Q, \tag{6}$$

where $\tilde{\mu}(\rho)$, γ, $D_Q, \sigma_Q > 0$, $|\boldsymbol{Q}|^2 = \sum_{\alpha\beta}\boldsymbol{Q}_{\alpha\beta}^2$, $\widehat{\nabla\nabla} = \nabla\nabla - \frac{1}{2}\nabla^2$, and $\boldsymbol{\eta}_Q$ is a symmetric traceless tensor whose components are unit Gaussian white noises. Upon replacing the activity A with the density ρ on the right-hand side of Eq. (6), one recovers the standard dynamics for active nematics [31,57].

We now estimate density fluctuations deep in the nematically ordered phase, that is, for $\rho = \rho_0$, such that $\tilde{\mu}(\rho_0) = \mu_0 > 0$ (and not small), using a linearized theory. Neglecting noises, Eqs. (4)–(6) admit a set of homogeneous solutions with $A = (\kappa\rho_0 - a)/\lambda = A_0 \propto \Delta\phi$, $S = \sqrt{2\mu_0/\gamma} = S_0$, and arbitrary nematic director $\boldsymbol{n}_0$ such that $\boldsymbol{Q}_0 = S_0(\boldsymbol{n}_0\boldsymbol{n}_0 - \frac{1}{2}\mathbf{1})$ [57]. We assume this homogeneous state to be linearly stable, which implicitly imposes conditions on the parameter values. In the presence of noise, we then consider small fluctuations of the density $\rho(\boldsymbol{r},t) = \rho_0 + \delta\rho(\boldsymbol{r},t)$, of the activity $A(\boldsymbol{r},t) = A_0 + \delta A(\boldsymbol{r},t)$, and of the nematic order $\boldsymbol{Q}(\boldsymbol{r},t) = \boldsymbol{Q}_0 + \delta\boldsymbol{Q}(\boldsymbol{r},t)$. Linearizing Eqs. (4)–(6) and introducing the spatial Fourier transform $\delta\hat{\rho}(\boldsymbol{q},t) = \int d\boldsymbol{r}\delta\rho(\boldsymbol{r},t)\exp[-i\boldsymbol{r}\cdot\boldsymbol{q}]$ with $\boldsymbol{q} = q(\cos\theta\boldsymbol{n}_0 + \sin\theta\boldsymbol{n}_\perp)$ and $\boldsymbol{n}_\perp\cdot\boldsymbol{n}_0 = 0$, one finds for the structure factor $S(\boldsymbol{q}) = \langle\delta\hat{\rho}(\boldsymbol{q},t)\delta\hat{\rho}(-\boldsymbol{q},t)\rangle$ the critical scaling behavior [55]

$$\frac{S(\boldsymbol{q})}{\Delta\phi^{1/2}} \propto \frac{(1-\cos 4\theta)\lambda^2\chi_2^2\sigma_Q^2}{D_Q D_\rho\kappa(\kappa D_\rho + \lambda D_Q)}\frac{1}{\tilde{q}^2} + \frac{2D_\rho\sigma_A^2}{\kappa\lambda}\tilde{q}^2, \tag{7}$$

where $\tilde{q} = q\xi$, with a crossover length $\xi = \Delta\phi^{-3/4}$. In this scaling regime, we thus observe a crossover between GNFs ($\lambda = -2$) for $q \ll q^* \sim \xi^{-1}$ and hyperuniformity ($\lambda = 2$) for $q \gg q^*$. The predicted values $\zeta' = \frac{1}{2}$ and $\mu = \frac{3}{4}$ are reasonably close to the measured $\zeta' \approx 0.55$ and $\mu \approx 0.625$, meaning that the linearized theory already captures a significant part of the phenomenology.

An intuitive understanding of this crossover behavior may be gained as follows. In the large length-scale regime $q \ll A_0^{1/2}$, the long timescale dynamics of a density mode $\delta\hat{\rho}(\boldsymbol{q},t)$ may be approximated as [55]

$$\partial_t\delta\hat{\rho} = -Dq^2\delta\hat{\rho} + \frac{\tilde{\sigma}_A q^2}{\sqrt{A_0}}\hat{\eta}_A + \tilde{\sigma}_Q\sin 2\theta A_0\hat{\eta}_Q^\perp, \tag{8}$$

with $D = D_\rho\kappa/\lambda$, $\tilde{\sigma}_A = D_\rho\sigma_A/\lambda$, $\tilde{\sigma}_Q = \chi_2\sigma_Q/D_Q$, and $\hat{\eta}_Q^\perp = \boldsymbol{n}_0\cdot\hat{\boldsymbol{\eta}}_Q\cdot\boldsymbol{n}_\perp$. We assumed for simplicity that $\chi_3 = 0$, as χ_3 plays no role in Eq. (7). The dynamics of $\delta\hat{\rho}$ is thus a (complex) Langevin equation with two effective noise terms: a "superconservative" noise of amplitude $\propto q^4/A_0$ induced by the activity field A, and a seemingly nonconserved noise of amplitude $\propto A_0^2$ induced by the nematic field $\boldsymbol{Q}$. Notably, the amplitudes of these two noises become comparable for $q^* \sim A_0^{3/4}$. The conserved noise ($\hat{\boldsymbol{\eta}}_\rho$ term) of amplitude $\propto q^2 A_0$ obtained from linearizing Eq. (4) is negligible in this regime. The noise $\hat{\eta}_A$ dominates over the noise $\hat{\eta}_Q^\perp$ for $q \gg q^*$ (intermediate scales) leading to the hyperuniformlike scaling $S(q) \sim q^2/A_0$. The noise $\hat{\eta}_Q^\perp$ instead dominates for $q \ll q^*$ (larger scales), where one obtains $S(q) \sim (1-\cos 4\theta)A_0^2/q^2$. Both results are in agreement with Eq. (7) (recalling that $A_0 \sim \Delta\phi$) and allow us to rationalize, at a heuristic level, the critical crossover as originating from the competition of two effective noise sources, each dominating on different length scales.

In this Letter, we have shown that systems of nematic active particles with a diffusivity activated by the presence of neighboring particles display an absorbing phase transition with unusual properties. Close to the transition, density fluctuations are suppressed at intermediate length scales, but enhanced on large length scales. The crossover length diverges as a power law of the distance to the transition point, and is thus a critical property, as also confirmed by a critical data collapse on both the number fluctuations and the structure factor. We rationalize this behavior, at a qualitative level, by deriving the structure factor from a linearized continuum theory. Our linearized theory captures the critical crossover between anomalous behaviors. At intermediate length scales, an effective noise, arising from the coupling with the activity field, controls and suppresses density fluctuations. At large length scales, density fluctuations are instead dominated by an effective noise arising from the coupling with the nematic tensor leading to GNFs. Interestingly, the behavior of density fluctuations is the opposite of the one observed in clustering or coarsening patterns in scalar active matter, where large density fluctuations occur on intermediate length scales, the system being hyperuniform on the largest length scales [28,29].

Our work opens avenues for the investigation of absorbing phase transitions in orientationally ordered active matter with environment-dependent motility, with experimental realizations ranging from suspensions of rods under cyclic shear [40,41] to Quincke rollers with neighbor-triggered motility [42], or to microrobots that can sense their neighborhood and modify their behavior accordingly [47,48]. On the numerical side, future work may try to quantitatively characterize the anisotropic features of the structure factor, beyond angular averages. On the theoretical side, whether the presence of orientational order modifies the activity-related critical exponents of the absorbing phase transition of the ROM, which corresponds to Conserved Directed Percolation (CDP) in the absence of orientational order [58], remains an important open question, which requires either extensive numerical simulations or the development of renormalization schemes for continuum equations coupling activity, nematic (or polar) and particle density fields.

S.D.C. acknowledges support from the LABS, Grant No. ANR-18-CE30-0028-01.

[1] L. Berthier, P. Chaudhuri, C. Coulais, O. Dauchot, and P. Sollich, Phys. Rev. Lett. **106**, 120601 (2011).
[2] C. E. Zachary, Y. Jiao, and S. Torquato, Phys. Rev. Lett. **106**, 178001 (2011).
[3] J. Ricouvier, R. Pierrat, R. Carminati, P. Tabeling, and P. Yazhgur, Phys. Rev. Lett. **119**, 208001 (2017).
[4] Z. Ma, E. Lomba, and S. Torquato, Phys. Rev. Lett. **125**, 068002 (2020).
[5] S. Torquato and F. H. Stillinger, Phys. Rev. E **68**, 041113 (2003).
[6] S. Torquato, Phys. Rep. **745**, 1 (2018).
[7] Z. Ma and S. Torquato, Phys. Rev. E **99**, 022115 (2019).
[8] S. Torquato, Phys. Rev. E **103**, 052126 (2021).
[9] D. Hexner and D. Levine, Phys. Rev. Lett. **114**, 110602 (2015).
[10] E. Tjhung and L. Berthier, Phys. Rev. Lett. **114**, 148301 (2015).
[11] K. J. Schrenk and D. Frenkel, J. Chem. Phys. **143**, 241103 (2015).
[12] J. H. Weijs, R. Jeanneret, R. Dreyfus, and D. Bartolo, Phys. Rev. Lett. **115**, 108301 (2015).
[13] D. Hexner and D. Levine, Phys. Rev. Lett. **118**, 020601 (2017).
[14] D. Hexner, P. M. Chaikin, and D. Levine, Proc. Natl. Acad. Sci. USA **114**, 4294 (2017).
[15] X. Ma, J. Pausch, and M. E. Cates, arXiv:2310.17391.
[16] R. Mari, E. Bertin, and C. Nardini, Phys. Rev. E **105**, L032602 (2022).
[17] L. Corté, P. M. Chaikin, J. P. Gollub, and D. J. Pine, Nat. Phys. **4**, 420 (2008).
[18] E. Tjhung and L. Berthier, J. Stat. Mech. (2016) 033501.
[19] J. Wang, J. M. Schwarz, and J. D. Paulsen, Nat. Commun. **9**, 2836 (2018).
[20] L. Milz and M. Schmiedeberg, Phys. Rev. E **88**, 062308 (2013).
[21] Q.-L. Lei and R. Ni, Proc. Natl. Acad. Sci. USA **116**, 22983 (2019).
[22] Q.-L. Lei, M. P. Ciamarra, and R. Ni, Sci. Adv. **5**, eaau7423 (2019).
[23] A. Fernandez-Nieves, A. de la Cotte, D. Pearce, J. Nambisan, A. Levy, and L. Giomi (unpublished).
[24] M. Huang, W. Hu, S. Yang, Q.-X. Liu, and H. P. Zhang, Proc. Natl. Acad. Sci. USA **118**, e2100493118 (2021).
[25] N. Oppenheimer, D. Stein, M. Zion, and M. Shelley, Nat. Commun. **13**, 804 (2022).
[26] R. Backofen, A. Y. A. Altawil, M. Salvalaglio, and A. Voigt, Proc. Natl. Acad. Sci. USA **121**, e2320719121 (2024).
[27] H.-H. Boltz and T. Ihle, arXiv:2402.19451.
[28] Y. Zheng, M. A. Klatt, and H. Löwen, Phys. Rev. Res. **6**, L032056 (2024).
[29] B. Zhang and A. Snezhko, Phys. Rev. Lett. **128**, 218002 (2022).
[30] F. D. Luca, X. Ma, C. Nardini, and M. E. Cates, J. Phys.: Condens. Matter **36**, 405101 (2024).
[31] S. Ramaswamy, R. Aditi Simha, and J. Toner, Europhys. Lett. **62**, 196 (2003).
[32] J. Toner, *Active Matter and Nonequilibrium Statistical Physics: Lecture Notes of the Les Houches Summer School: Volume 112, September 2018*, edited by J. Tailleur, G. Gompper, M. C. Marchetti, J. M. Yeomans, and C. Salomon (Oxford University Press, Oxford, UK, 2022), p. 52.
[33] H. Chaté, F. Ginelli, and R. Montagne, Phys. Rev. Lett. **96**, 180602 (2006).
[34] S. Dey, D. Das, and R. Rajesh, Phys. Rev. Lett. **108**, 238001 (2012).
[35] S. Ngo, A. Peshkov, I. S. Aranson, E. Bertin, F. Ginelli, and H. Chaté, Phys. Rev. Lett. **113**, 038302 (2014).
[36] V. Narayan, S. Ramaswamy, and N. Menon, Science **317**, 105 (2007).
[37] J. Deseigne, O. Dauchot, and H. Chaté, Phys. Rev. Lett. **105**, 098001 (2010).
[38] H. P. Zhang, A. Be'er, E.-L. Florin, and H. L. Swinney, Proc. Natl. Acad. Sci. USA **107**, 13626 (2010).
[39] F. Giavazzi, C. Malinverno, S. Corallino, F. Ginelli, G. Scita, and R. Cerbino, J. Phys. D: Appl. Phys. **50**, 384003 (2017).
[40] A. Franceschini, E. Filippidi, E. Guazzelli, and D. J. Pine, Soft Matter **10**, 6722 (2014).
[41] M. Trulsson, Phys. Rev. E **104**, 044614 (2021).
[42] Z. T. Liu, Y. Shi, Y. Zhao, H. Chaté, X.-q. Shi, and T. H. Zhang, Proc. Natl. Acad. Sci. USA **118**, e2104724118 (2021).
[43] S. Vedel, S. Tay, D. Johnston, H. Bruus, and S. Quake, Proc. Natl. Acad. Sci. USA **110**, 129 (2013).
[44] T. Putelat, P. Recho, and L. Truskinovsky, Phys. Rev. E **97**, 012410 (2018).
[45] Y. Sumino, K. H. Nagai, Y. Shitaka, D. Tanaka, K. Yoshikawa, H. Chaté, and K. Oiwa, Nature (London) **483**, 448 (2012).
[46] J. Chen, X. Lei, Y. Xiang, M. Duan, X. Peng, and H. P. Zhang, Phys. Rev. Lett. **132**, 118301 (2024).
[47] S. Muiños-Landin, A. Fischer, V. Holubec, and F. Cichos, Sci. Robot. **6**, eabd9285 (2021).
[48] M. Y. Ben Zion, J. Fersula, N. Bredeche, and O. Dauchot, Sci. Robot. **8**, eabo6140 (2023).

[49] This particular choice ensures that the absorbing phase transition occurs near $\rho = 2$, for which the active nematics study of [35] was performed. Other choices are possible—see, e.g., for $\sigma = 0.05$, $\delta_0 = 0.3$, $R_{\rm al} = 1$, and $D = 0.3$ [55].
[50] S. Lübeck, Int. J. Mod. Phys. B **18**, 3977 (2004).
[51] G. I. Menon and S. Ramaswamy, Phys. Rev. E **79**, 061108 (2009).
[52] S. Bub Lee, J. Stat. Mech. (2019) 053201.
[53] S. Wilken, R. E. Guerra, D. J. Pine, and P. M. Chaikin, Phys. Rev. Lett. **125**, 148001 (2020).
[54] S. S. Manna, J. Phys. A: Math. Gen. **24**, L363 (1991).
[55] See Supplemental Material at http://link.aps.org/supplemental/10.1103/m6bl-dqsd for a full derivation of Eqs. (7) and (8) and for complementary numerical datas, which also contains Refs. [57–59].
[56] R. Pastor-Satorras and A. Vespignani, Phys. Rev. E **62**, R5875 (2000).
[57] E. Bertin, H. Chaté, F. Ginelli, S. Mishra, A. Peshkov, and S. Ramaswamy, New J. Phys. **15**, 085032 (2013).
[58] H. Hinrichsen, Adv. Phys. **49**, 815 (2000).
[59] S. Henkes, K. Kostanjevec, J. M. Collinson, R. Sknepnek, and E. Bertin, Nat. Commun. **11**, 1405 (2020).